

# 1 **European sulphate aerosols were a key driver of the early** 2 **twentieth-century intensification of the Asian summer monsoon**

3  
4 Weihao Sun<sup>1,2</sup>, Massimo A. Bollasina<sup>1</sup>, Ioana Colfescu<sup>3,4</sup>, Guoxiong Wu<sup>2</sup> and Yimin Liu<sup>2</sup>  
5

6 <sup>1</sup>East China Sea Forecasting and Disaster Reduction Center, Ministry of Natural Resources, Shanghai, China

7 <sup>2</sup>Observation and Research Station of Huaniaoshan East China Sea Ocean-Atmosphere Integrated Ecosystem,  
8 Ministry of Natural Resources, Shanghai, China

9 <sup>3</sup>School of Mathematics and Statistics, University of St Andrews, St Andrews, UK

10 <sup>4</sup>National Centre for Atmospheric Science, UK  
11  
12

13 Correspondence to: Massimo A. Bollasina ([Massimo.Bollasina@ed.ac.uk](mailto:Massimo.Bollasina@ed.ac.uk))  
14  
15

16 **Abstract.** Observations show that the Asian summer monsoon experienced substantial multi-decadal changes  
17 during the early 20<sup>th</sup> century, including a wetting trend over South Asia and a southward rainfall shift over East  
18 Asia. Despite their significance, these variations have received limited attention, and the underlying mechanisms  
19 remain poorly understood. This study investigates the role of increased European sulphate aerosol emissions in  
20 shaping these monsoon changes using ensemble experiments with the Community Earth System Model. The  
21 aerosol-driven rainfall patterns over South and East Asia resemble observations, suggesting that European  
22 aerosols played an important role in modulating the monsoon. These changes are linked to large-scale anomalies  
23 in surface climate and three-dimensional atmospheric circulation across the Indo-Pacific, which alter moisture  
24 transport to the continent, the main driver of the rainfall anomalies. Regional circulation anomalies form part of a  
25 hemispheric upper-tropospheric wave train originating over central Europe and extending through the Middle East  
26 to the Pacific. The wave train arises as a thermodynamic adjustment to the aerosol-induced surface cooling and  
27 related anticyclone over Europe, extends to the upper troposphere, and, while propagating eastward, induces three-  
28 dimensional circulation anomalies across Asia that affect the monsoon. These findings provide compelling  
29 evidence for the influence of European sulphate aerosols on the early 20<sup>th</sup>-century monsoon variability, which is  
30 relevant for improving current understanding of the regional-scale impacts of anthropogenic aerosols. As  
31 European SO<sub>2</sub> emissions continue to decline, this study sheds light upon a possible ongoing and future pathway  
32 which may significantly modulate the monsoon response to Asian aerosol changes.

## 33 **1 Introduction**

34 The Asian summer monsoon (ASM) is a vital source of water for over 60% of the world's population (Turner and  
35 Annamalai, 2012). Its interannual variability and long-term changes have significant implications for water  
36 resources, agriculture, and economic activities across Asia (e.g., Gadgil and Rupa Kumar, 2006).

37

38 In the past decade, anthropogenic aerosols have attracted considerable scientific interest due to their ability to  
39 offset part of the warming caused by greenhouse gases (GHGs) (e.g., Samset et al., 2018; Hegerl et al., 2019; Li  
40 et al., 2022). Aerosols influence climate by scattering and absorbing solar radiation, and by acting as cloud  
41 condensation and ice nuclei, thereby modifying cloud albedo, lifetime, and precipitation processes (Boucher et  
42 al., 2013; Stier et al., 2024). They remain the largest source of uncertainty in estimating anthropogenic climate  
43 forcing since the pre-industrial era (Andrews and Forster, 2020; Bellouin et al., 2020). While their global historical  
44 effective radiative forcing is smaller than that of GHGs, aerosols can trigger strong regional climate responses due  
45 to their spatial and temporal variability (e.g., Szopa et al., 2021).

46

47 The link between long-term changes in aerosol emissions and ASM variability is widely debated (e.g., Lau 2016;  
48 Li et al., 2016; Wu et al., 2016). Research is particularly challenging due to the compounding effects of internal  
49 variability, model biases, and divergent model responses (e.g., Saha and Gosh, 2019; Liu et al., 2024).  
50 Nonetheless, studies using observational and modelling evidence have highlighted the significant impact of  
51 aerosols, both regional (i.e., Asian-only) and remote (i.e., outside Asia), on the late 20<sup>th</sup> century weakening of the  
52 South ASM and the emergence of a southern-flood-northern-drought (SFND) pattern over East Asia (e.g.,  
53 Bollasina et al., 2011; Guo et al., 2013; Salzmänn et al., 2014; Li et al., 2015; Dong et al. 2019; Wilcox et al.  
54 2020).

55

56 Gauge records reveal clear multi-decadal variability in both South Asian and East Asian summer monsoons  
57 throughout the 20<sup>th</sup> century (e.g., Zhang and Zhou, 2011; Preethi et al., 2017; Li et al., 2023). In particular, the  
58 first half of the century saw an increase in rainfall over South Asia, most notably in central India, and a tripole  
59 pattern over East Asia, with excess rainfall in the south and northeast, and drier conditions along the Yangtze River  
60 basin. These anomalies appear to be part of a coherent ASM-wide fluctuation, mirrored in broader Northern  
61 Hemispheric summer monsoon changes (Zhang and Zhou, 2011; Preethi et al., 2017; Wang et al., 2018; Goswami

62 et al., 2023). Strikingly, this pattern reversed in the second half of the 20<sup>th</sup> century, producing comparable but  
63 opposite sign anomalies, and resulting in minimal net change over the full period.

64

65 While monsoon changes since the 1950s have been extensively studied (e.g., Bollasina et al., 2011; Salzmann et  
66 al., 2014; Song et al., 2014; Liu et al., 2019; Liu et al., 2024; Shao et al., 2024), early-century variations have  
67 received less attention. Yet, given the contrasting trends throughout the historical period, understanding monsoon  
68 drivers and the underpinning physical mechanisms in the entire record is essential to constrain the nature of its  
69 multi-decadal variability and improve future projections. This is particularly relevant in the context of  
70 disentangling internal climate variability from externally-forced changes (e.g., Salzmann and Cherian, 2015;  
71 Huang et al., 2020). In this regard, compared to the later period, it is conceivable to assume a negligible role of  
72 Asian aerosols in the first half of the 20<sup>th</sup> century, as emissions underwent a significant growth only from the  
73 1950s and a sharp rise after the 1970s (Smith et al., 2011; Lund et al., 2019). In contrast, North American and  
74 European aerosols had already increased substantially, raising the possibility of their significant influence on the  
75 monsoon.

76

77 Several studies have highlighted the potential role of remote, including European, aerosols in driving Asian  
78 summer monsoon changes (e.g., Cowan and Cai, 2011; Bollasina et al., 2014; Guo et al., 2015; Dong et al., 2016;  
79 Liu et al., 2018; Shawki et al., 2018; Undorf et al., 2018a,b; Westervelt et al., 2018; Wang et al., 2020). However,  
80 these analyses often relied on idealised simulations, such as long equilibrium experiments with present-day  
81 emissions turned on or off. Whether aerosol influences were already detectable in the early 20<sup>th</sup> century remains  
82 an open question. Addressing this gap is crucial for better understanding and narrowing uncertainty in aerosol-  
83 related future monsoon projections, especially considering divergent present-day emission trends (e.g., Wang et  
84 al., 2021a) and a wide range of plausible future pathways (Samset et al., 2019; Persad et al., 2023).

85

86 Against this backdrop, this study investigates whether rising European sulphate aerosols – the dominant  
87 anthropogenic aerosol species of the region (e.g., Hoesly et al., 2018) – had any detectable impact on the ASM  
88 during the first half of the 20<sup>th</sup> century. Section 2 introduces the climate model, experimental setup, and  
89 observational data used. Section 3 presents the ASM response and examines the underlying mechanism.  
90 Discussion and conclusions are provided in Section 4.

91 **2 Data and methods**

92 The primary data comprises output from two transient historical (1850–2005) experiments with the fully coupled  
93 Community Earth System Model (CESM) version 1.2.2 (Hurrell et al., 2013). The atmospheric component is the  
94 Community Atmospheric Model version 5.3 (CAM5.3, Neale et al., 2012), which includes a 3-mode aerosol  
95 scheme and a prognostic representation of aerosol-cloud interactions (Ghan et al., 2012). The horizontal  
96 resolutions are  $1.9^\circ \times 2.5^\circ$  for the atmosphere and  $0.6^\circ \times 0.9^\circ$  for the ocean. The model reproduces spatial patterns  
97 and magnitude of the climatological summertime monsoon rainfall and low-tropospheric circulation reasonably  
98 well (Supplementary Figure S1), consistent with the overall performance of CMIP5/CMIP6 models (Meehl et al.,  
99 2020; He et al., 2023). A full description of the model and experiments is provided by Undorf et al. (2018a); here,  
100 we briefly summarise key details.

101  
102 Each experiment consists of an 8-member ensemble initialised from different points in a 200-year pre-industrial  
103 (PI) simulation with fixed anthropogenic emissions at 1850 levels. The first experiment (ALL) includes time-  
104 varying historical emissions of anthropogenic aerosols, greenhouse gases, and natural forcing factors. The second  
105 (fixEU) is identical to ALL except that anthropogenic  $\text{SO}_2$  and  $\text{SO}_4$  emissions over Europe (EU) are held at PI  
106 levels. Europe is defined according to Tier 1 regions from the Hemispheric Transport of Air Pollution 2  
107 experiments (Koffi et al., 2016).

108  
109 Several observational datasets are also used. Precipitation was taken from three land-only monthly gridded gauge-  
110 based datasets to account for uncertainties and discrepancies: the  $1^\circ \times 1^\circ$  Global Precipitation Climatology Centre  
111 v2020 (GPCC; Schneider et al., 2014), the  $0.5^\circ \times 0.5^\circ$  Climate Research Unit v4.00 (CRU; Harris et al., 2014),  
112 and the  $0.5^\circ \times 0.5^\circ$  University of Delaware v401 (UDEL, Willmott and Matsuura, 1995). Monthly sea level  
113 pressure surface is from the  $5^\circ \times 5^\circ$  Hadley Centre Sea Level Pressure dataset (HadSLP2; Allan and Ansell, 2006),  
114 and 850-hPa winds from the ECMWF Reanalysis 5 (Hersbach et al., 2020). Monthly observed precipitation from  
115 the  $2.5^\circ \times 2.5^\circ$  Climate Prediction Center Merged Analysis of Precipitation dataset (CMAP, Xie and Arkin, 2017)  
116 is also used for model validation.

117  
118 The analysis focuses on the summer (June–August, JJA) monsoon variation during the early 20<sup>th</sup> century.  
119 Temporal changes are estimated using least-squares linear trends from 1901 to 1955. Alternative trend estimation

120 methods (i.e., Sen's non-parametric slope or differences between the 1941–1955 and 1901–1915 means) yield  
121 similar results (not shown). As the main objective is to isolate the influence of external forcing, particularly  
122 anthropogenic aerosols, on the ASM, changes are primarily assessed using ensemble means. Assuming linear  
123 additivity of responses, the difference between the ALL and fixEU experiments is interpreted as the impact of  
124 European SO<sub>2</sub> emissions. Statistical significance is assessed using a two-tailed Student's *t*-test at the 90%  
125 confidence level. To identify the contribution of the model's internal variability to the forced response, individual  
126 ensemble members are also examined. Additionally, the PI simulation is used to assess the statistical significance  
127 of the forced changes relative to internal variability. We generate 10,000 bootstrap samples of 8-member ensemble  
128 means to construct the probability distribution of unforced linear trends; the 90% confidence interval is defined  
129 as the range within which 90% of these fall.

### 130 **3 Results**

#### 131 **3.1 Observed and simulated precipitation trends**

132 Observational data show that JJA precipitation changes across Asia during the first half of the twentieth century  
133 exhibit a coherent large-scale pattern (Figure 1a), with robust features across multiple datasets (Supplementary  
134 Figure S2). Over South Asia, significant wetting is observed across central and northern India, contrasted by  
135 drying over southern and northeastern India, the eastern Himalayas and northern Myanmar. Further east, rainfall  
136 deficits occur over southern Indochina and Indonesia, with a pronounced drying over the middle and lower reaches  
137 of the Yangtze River valley (105°–120°E, 25°–35°N). In contrast, precipitation increases are seen in a band  
138 extending from northern Indochina through southern China, and further north into northwestern China and the  
139 Korean peninsula. Interestingly, the anomalous rainfall pattern over South Asia closely resembles, but with  
140 opposite sign, that associated with the late 20<sup>th</sup> century weakening of the monsoon, while the anomalies over  
141 eastern Asia are reminiscent of the reversed SFND pattern (e.g., BOLLASINA et al., 2011; Dong et al., 2016).

142

143 To provide further context on the long-term precipitation variations, Figure 1c shows the observed time series of  
144 monsoon rainfall anomalies over the core Indian monsoon region (75°–87°E, 16°–27°N land-only points, see box  
145 in Figure 1c). Beyond interannual and decadal fluctuations, the record reveals a marked increase from the 1900s  
146 to the mid-1950s (+0.55/+0.76 mm day<sup>-1</sup> in GPCC/CRU over 55 years, statistically significant at the 90%  
147 confidence level), equivalent to about 7–11% of the long-term climatology. The anomaly also results in a 5–7%

148 increase in the All-India rainfall relative to early-century values. A similar analysis over southern China (110°–  
149 120°E, 25°–35°N; Supplementary Figure S3) also shows a prominent, statistically significant, multi-decadal trend.

150

151 Despite its coarser resolution, the ALL ensemble mean captures the main spatio-temporal characteristics of the  
152 observed precipitation trends, although amounts are generally smaller (Figure 1b). The model reproduces the  
153 observed widespread precipitation increase over northern India, albeit with a weaker magnitude ( $+0.14 \text{ mm day}^{-1}$   
154  $(55 \text{ years})^{-1}$  over the core region) and a slight eastward shift, and the drying over southern India. The model likely  
155 underrepresents the full extent of the interaction with the Western Ghats. The simulated rainfall dipole over eastern  
156 China aligns with observations, although the amounts are slightly underestimated. However, the model fails to  
157 reproduce the observed wetting over southern China and northern Indochina, possibly due to limitations in  
158 resolving interactions with the complex terrain. The sign of the core precipitation anomalies over India is  
159 consistent across most of the individual ensemble members (6 out of 8), supporting a dominant anthropogenic  
160 origin (Supplementary Figure S4).

161

162 Preventing European sulphate aerosols from increasing results in drier conditions over central-northern India and  
163 the northern Bay of Bengal (BoB), with wetting over the eastern Himalayas and Myanmar. Concurrently, the  
164 precipitation anomalies over eastern Asia reverse polarity, while a pronounced precipitation deficit appears over  
165 Indochina. As a result, the precipitation pattern associated with increased European  $\text{SO}_2$  emissions closely  
166 resembles observations and shows greater similarity than ALL across Asia. The aerosol-related precipitation  
167 response is also robust across most of the ensemble members (Supplementary Figure S4). For example, the  
168 ensemble-mean rainfall trend over the core Indian region amounts to  $+0.33 \text{ mm day}^{-1}$  over 55 years, with increases  
169 in 6 out of 8 ensemble members. This indicates that European aerosols substantially contributed to the early 20<sup>th</sup>-  
170 century ASM rainfall trends.

171

172 The observed and simulated 55-year rainfall trends over central-northern India are also compared with the  
173 corresponding range of trends from the PI experiment (Supplementary Figure S4)). The trend from CRU is outside  
174 the respective 90% confidence interval, while it is slightly below in GPCC. The trend from the ALL-ensemble  
175 mean is within the corresponding 90% confidence interval ( $+0.19 \text{ mm day}^{-1}$  over 55 years; Supplementary Figure  
176 S5), although five of its members exhibit positive trends that are markedly discernible from internal variability.

177 The ensemble-mean drying trend in the fixEU experiment exceeds the 90% confidence level. As a result, the  
178 ensemble-mean trend associated with European aerosols (EU) is clearly distinguishable from internally-generated  
179 fluctuations, even exceeding the 95% confidence level (+0.24 mm day<sup>-1</sup> over 55 years).

### 180 **3.2 Changes in the monsoon circulation**

181 Changes in precipitation across Asia are closely linked with variations in near-surface and atmospheric circulation  
182 patterns (Figure 2). The spatial correspondence between wet (dry) anomalies and regions of moisture flux  
183 convergence (divergence) underscores the dominant role of circulation-induced moisture transport in shaping  
184 monsoon precipitation trends (Figure 2b). Over South Asia, a prominent anomalous anticyclone centred over  
185 southern India and the western BoB characterises the low-tropospheric flow. Over East Asia and the western  
186 Pacific, a zonal dipole emerges: an anomalous cyclone spans northern Indochina, southeastern China, and the  
187 South China Sea, accompanied by an elongated anticyclone extending from central China to the western Pacific.

188

189 As Figure 2a shows, strong low-level easterlies across southern India oppose the climatological westerlies from  
190 the Arabian Sea, leading to local rainfall deficits. Meanwhile, the climatological moisture-laden southwesterlies  
191 are deflected northward over the northern Arabian Sea. Upon reaching central and northern India, this flow  
192 converges with anomalous northeasterlies from northern Indochina and the northern BoB, enhancing rainfall  
193 (Figure 2b). On the western flank of the anomalous Indo-Pakistan low, dry northerlies suppress precipitation over  
194 Pakistan. Over East Asia, enhanced Pacific moisture transport into southern China and northeastern Indochina,  
195 opposing the climatological southerlies linked to the western Pacific subtropical high, leads to regional wetting.  
196 Return westerlies south of the anomalous Pacific low further reinforce the moisture flux from the BoB,  
197 contributing to widespread wetting across the Bay and northwestern Indochina. In contrast, reduced southerly  
198 moisture advection brings drying to southern Indonesia and northeastern China.

199

200 Figure 2c shows that the regional upper-tropospheric circulation also exhibits substantial changes, consistent with  
201 the tropical balance among convective heating, ascent, and upper-level divergence (and vice versa). Over northern  
202 India and the northern BoB, strong mid-tropospheric ascent coincides with rainfall enhancement, accompanied by  
203 divergent outflow in the upper troposphere. One branch heads northeastward, converging and subsiding over  
204 Burma and central China. Other branches are directed southwestward and southward, with corresponding mid-  
205 tropospheric subsidence and surface anticyclones over southern India and the northern equatorial Maritime

206 Continent. A meridional system of divergent cells over East Asia and the western Pacific reflects the deep  
207 convection and upper-tropospheric divergence centred near 20°N. The southern cell also converges and subsides  
208 over the north equatorial Maritime Continent, aligning with the southern outflow from South Asia.

### 209 **3.3 Aerosol forcing over Europe**

210 To elucidate the generating mechanism, Figure 3a shows the widespread sulphate loading anomaly over Europe  
211 resulting from enhanced emissions. Once emitted, aerosols are transported across and beyond the Continent.  
212 Notably, aerosols spread southwestward towards northern Africa and the tropical Atlantic via the summertime  
213 climatological circulation of the Azores high, and eastward over central Eurasia by the midlatitude climatological  
214 westerlies, displacing the maximum loading and Aerosol Optical Depth (AOD; Supplementary Figure S6)  
215 eastward of the emissions source.

216

217 Consistent with this transport, surface clear-sky downward shortwave radiation decreases across Europe, with  
218 anomalies exceeding  $-3 \text{ W m}^{-2}$  over 55 years in regions of peak aerosol loading (Figure 3b), accounting for  
219 approximately 80% of the local reduction in the all-sky radiation (Supplementary Figure S6). All-sky radiation  
220 anomalies are larger (up to  $-5 \text{ W m}^{-2}$ ) due to increased cloudiness associated with circulation changes (see last  
221 paragraph in this Section). As expected by the aerosol scattering effect, net shortwave differences between the  
222 top-of-atmosphere and surface are minimal (Supplementary Figure S6). Including longwave effects, the net  
223 radiative cooling at the model top reached about  $-2 \text{ W m}^{-2}$  over central and eastern Europe (Supplementary Figure  
224 S6).

225

226 Cloud droplet number concentration displays widespread positive anomalies over central and eastern Europe  
227 concurrently with a negative, albeit weak, decrease in cloud top effective radius (Supplementary Figure S6). These  
228 changes are consistent with those expected by the cloud response to sulphate aerosols, assuming negligible  
229 variations in water liquid content. The latter remains relatively unchanged or slightly enhanced due to anomalous  
230 northwesterlies from the Atlantic (see next paragraph).

231

232 As a result of the aerosol-induced dimming, near-surface temperature shows anomalous cooling over central and  
233 eastern Europe (Figure 3c), and concurrently, the circulation adjusts thermodynamically, with marked anticyclonic  
234 anomalies occurring at the surface. Interestingly, Figure 3d shows that the largest cooling and the high-pressure

235 core are displaced east of the aerosol loading maximum, suggesting the combined influence of direct forcing,  
236 feedbacks, and modulation by the climatological flow. For example, eastward aerosol transport and temperature  
237 advection by the climatological westerlies contribute in concert to displacing the aerosol cooling to the east. The  
238 associated northeasterly flow on the eastern flank of the surface anticyclone further reinforces the cooling over  
239 eastern Europe. Note that the simulated northeastward displacement of the anomalous anticyclone is consistent  
240 with the displacement shown by observed sea-level pressure trends (Supplementary Figure S7).

### 241 **3.4 Rossby wave propagation and remote teleconnections**

242 As shown in Figure 4, the regional signature of European aerosols extends to the mid and upper troposphere.  
243 Streamfunction anomalies feature a (weak) equivalent-barotropic nature and a slight northwestward tilt with  
244 height (not shown), consistent with the mature phase of an extratropical disturbance. At 300 hPa, anticyclonic  
245 anomalies are seen over central Europe. This pattern forms part of a wave train signal extending across the  
246 northern hemisphere, indicating a Rossby wave response to increased European aerosols and related upper-level  
247 relative vorticity anomalies, which serve as the primary source of wave activity.

248

249 Upper-level meridional wind anomalies align with expectations from the streamfunction/geopotential height  
250 pattern, revealing alternating cyclonic and anticyclonic centres (Figure 4b). The wave activity flux (e.g., Takaya  
251 and Nakamura 2001) highlights two eastward propagation branches. The main branch extends southeastward  
252 across the Middle East to Pakistan and northwestern India, where it weakens while turning northeastward into  
253 eastern China and converges over Japan. This flux follows the Asian jet stream, which acts as a Rossby waveguide.  
254 A secondary, weaker high-latitude pathway is also evident: the wave flux points northeastward towards northern  
255 Russia, crosses northern Eurasia, and then turns southeastward over the northwestern Pacific, ultimately  
256 converging with the main pathway.

257

258 Mid-tropospheric ascent and descent anomalies accompany the wave train (Figure 4b), consistent with the  
259 vorticity balance (e.g., Rodwell and Hoskins 2001). For example, the anticyclonic anomaly over Afghanistan and  
260 Pakistan induces southward flow and subsidence to its east, suppressing precipitation over Pakistan and the  
261 western Tibetan Plateau. Conversely, an anomalous upper-tropospheric anticyclone develops over eastern China  
262 and the western Pacific (120°-140°E). Northward flow and ascent occur on its western flank, while subsidence is  
263 found to the east, in agreement with the fundamental vorticity balance. At lower levels, this configuration

264 generates an anomalous westerly flow from the western Pacific toward south-eastern China, enhancing moisture  
265 transport and producing a positive precipitation anomaly. This rainfall anomaly, in turn, drives strong variations  
266 in the tropical divergent circulation: part of the divergent outflow extends toward the Maritime Continent, where  
267 it converges, descends, and produces anomalous anticyclonic flow. The interaction between extratropical wave-  
268 induced anomalies over eastern China/western Pacific and the resulting meridional adjustments in the tropical  
269 divergent circulation account for the characteristic tripolar anomalous rainfall pattern across East Asia. These  
270 results suggest that key upper-tropospheric action centres, over the Middle East and southern China/western  
271 Pacific, initiate low-tropospheric circulation adjustments that generate the anomalous rainfall pattern across Asia.

#### 272 **4 Discussion and concluding remarks**

273 The Asian summer monsoon hydroclimate underwent significant changes in the early 20<sup>th</sup> century, characterised  
274 by a wetting trend over South Asia and a southern rainfall shift over East Asia. This study finds that increased  
275 European anthropogenic sulphate aerosols played a key role in driving these observed monsoon changes. The  
276 aerosol-induced cooling and large-scale anticyclonic anomaly over central/eastern Europe extend from the surface  
277 to the upper troposphere. These anomalies trigger subsequent atmospheric circulation adjustments in the form of  
278 an eastward propagating Rossby-wave train, which is central to realising the remote aerosol impact across Asia.

279

280 These findings shed new light on the drivers and mechanisms of monsoon multidecadal variability. While most  
281 existing research has focused on recent monsoon changes, the early historical period remains unexplored.  
282 Moreover, many prior studies have relied on long, equilibrium-type experiments to enhance the signal-to-noise  
283 ratio, but these are less representative of the transient response to evolving aerosol emissions. An atmospheric  
284 propagation pathway similar to the one identified here has been discussed in earlier literature, particularly in  
285 relation to the downstream signature of the North Atlantic Oscillation (e.g., Watanabe 2004) and broader  
286 teleconnections between Europe and East Asia (e.g., Lu et al. 2002; Enomoto et al., 2003), yet it has been largely  
287 overlooked in the context of aerosol forcing (e.g., Wang et al., 2021b), which has instead typically emphasised  
288 changes in the large-scale meridional temperature gradient across Eurasia as the dominant key mechanism.

289

290 Placing our study within the broader literature on remote aerosol-monsoon interactions underscores its relevance.

291 Cowan and Cai (2011) were among the first to identify the influence of non-Asian aerosols, primarily European

292 sulphate, in weakening the ASM over the 20<sup>th</sup> century by inducing widespread Eurasian cooling and thereby  
293 reducing the meridional temperature gradient, which in turn weakens the southerly monsoon flow. Similarly, Guo  
294 et al. (2015, 2016) linked widespread drying across Asia to increased global aerosol emissions, mainly from non-  
295 Asian sources, and the subsequent modulation of the zonal-mean meridional temperature gradient. Focusing on  
296 the fast, atmospheric-only equilibrium response to the removal of European aerosols, Dong et al. (2016) reported  
297 a strengthening of the South Asian monsoon and a southern shift in East Asian rainfall, attributed to the  
298 downstream advection of cooler, drier air from Europe to Asia and consequent weakening of the tropospheric  
299 thermal gradient. Shawki et al. (2018) similarly found that removing European aerosol emissions strengthens,  
300 albeit weakly, the South Asian monsoon and shifts the East Asian monsoon northward, via changes in the large-  
301 scale temperature gradient and the interhemispheric heat and moisture transport. Liu et al. (2018) reported a slight  
302 decrease in annual mean precipitation over Asia associated with increased European sulphate aerosols, driven by  
303 the slow (ocean-mediated) component of the total response via inter-hemispheric heating redistribution. Similar  
304 rainfall patterns were also shown by Westervelt et al. (2018). More recently, Wang et al. (2017) and Wang et al.  
305 (2020) highlighted that non-local aerosol emissions are as influential as local ones in weakening the East Asian  
306 summer monsoon, primarily through easterly advection of colder air across Eurasia and resulting change in  
307 meridional heat transport, in agreement with Dong et al. (2016).

308

309 An enhanced meridional temperature gradient between central Eurasia and the IO is a well-known contributor to  
310 stronger monsoon precipitation over South Asia (e.g., Meehl and Arblaster, 2002). Indeed, this has been identified,  
311 for example, as one of the elements contributing to enhanced future monsoon precipitation by the end of the 21<sup>st</sup>  
312 century (e.g., Meehl et al., 2024). This outcome, however, is not borne out in our study, as the mid and high  
313 troposphere temperature averaged over the 60°-100°E sector displays enhanced cooling compared to the north-  
314 equatorial IO, resulting in a weaker meridional temperature gradient (not shown). This discrepancy indicates that  
315 the aerosol-induced regional monsoon circulation and precipitation variations over South Asia cannot be explained  
316 by broad-scale sector-mean temperature changes. On the contrary, the anomalous temperature pattern over Eurasia  
317 displays a close relationship with that induced by the anomalies in atmospheric advection, especially in the  
318 meridional direction, in turn associated with the upper-tropospheric wave train.

319

320 This dynamical pathway and the critical role of large-scale remotely driven atmospheric dynamical changes finds

321 support in Bollasina et al. (2014). Although secondary to regional emissions in explaining the recent monsoon  
322 rainfall decline, extratropical aerosols were nonetheless shown to induce widespread temperature and wind  
323 anomalies across Asia, revealing the complex interplay between aerosol forcing, precipitation, and circulation  
324 changes. Undorf et al. (2018a, b) also highlighted the importance of midlatitude aerosol forcing in explaining the  
325 observed weakening of the South Asian monsoon through the mid-1970s, underscoring the key role of Eurasian-  
326 scale dynamical adjustments.

327

328 An important question is whether Indian Ocean (IO) SSTs also influenced the monsoon. The ALL ensemble,  
329 consistent with the overall performance of CMIP5/6 models (e.g., Roxy et al., 2014), exhibits widespread and  
330 relatively homogeneous warming across the basin. In contrast, aerosol-induced SST trends, albeit weak, show  
331 warming over the western equatorial IO and cooling over the subequatorial regions (Supplementary Figure S8).  
332 This cross-equatorial dipole in SST trends is also evident, and more pronounced, in observations (e.g., Figure 3  
333 in Goswami et al., 2023), which suggests an aerosol contribution to the IO warming pattern. Further analysis of  
334 the EU ensemble (Supplementary Figure S8), shows that SST anomalies are largely anticorrelated with  
335 evaporation: reduced evaporation dominates the western and equatorial IO, while increases are seen in the south.  
336 Concurrently, anomalous near-surface divergent easterlies across the north-equatorial IO oppose the  
337 climatological (south) westerlies, reducing evaporation and upwelling, which contribute to warming the SSTs.  
338 These patterns are similar to those associated with the Indian summer monsoon multi-decadal variability during  
339 the 20<sup>th</sup> century (Goswami et al., 2023). Also, the 55-year SST pattern resembles 20<sup>th</sup>-century-long changes,  
340 although the latter exhibits weaker anomalies and a less pronounced cooling (e.g., Rao et al., 2012; Roxy et al.,  
341 2014). Uncertainties remain in identifying the causes of the persistent western IO warming due to strong feedbacks  
342 between oceanic anomalies, atmospheric circulation, and convection (e.g., Rao et al., 2012; Swapna et al., 2014).  
343 While our findings highlight the role of remotely-forced wind anomalies, other mechanisms may also contribute.  
344 While SST anomalies and rainfall are anticorrelated in the long term, this relationship reverses in the early 20<sup>th</sup>  
345 century (Figure 3 in Roxy et al., 2015), aligning with our findings.

346

347 Our results have important implications. They suggest that non-local anthropogenic aerosols have contributed  
348 significantly to shaping monsoon variability even during the early historical period. This is particularly relevant  
349 for understanding regional-scale impacts of anthropogenic forcing, which remain uncertain due to the spatial

350 heterogeneity of emissions and their diverse climate effects. Importantly, under the current continued decrease in  
351 European aerosol emissions, assuming an opposite ASM response to the one described above, remotely-driven  
352 precipitation anomalies may significantly modulate, if not partially offset, the response to Asian aerosol emission  
353 changes (already declining or expected to do so in the future; e.g., Lund et al., 2019; Xiang et al. 2023). For  
354 example, assuming linearity in the combined responses, the abatement of EU sulphate aerosols would lead to a  
355 weaker monsoon over most of South Asia, and India in particular, which is opposite to the expected wetting  
356 associated with decreased sulphate aerosols over both South and East Asia (e.g., Bartlett et al., 2018). Conversely,  
357 EU aerosol reductions would contribute to further amplify the reversed SFND pattern over China brought about  
358 by decreased East Asian aerosol alone (e.g., Dong et al., 2016), resulting, for example, in enhanced drying over  
359 southeastern China. While the future monsoon response to the projected decline in worldwide aerosol emissions  
360 will most likely result from non-linear interactions among the different aerosol source regions, the above picture  
361 illustrates the complex interplay among local and remote aerosols and the need for a consistent and coordinated  
362 modelling and analysis approach (e.g., Wilcox et al., 2023).

363

364 While our analysis emphasises the central role of European aerosols, other remote emissions (e.g., from North  
365 America) and external forcings (e.g., greenhouse gases) may have also played a role. Our conclusions are based  
366 on ensemble experiments comprising eight members each, consistent with the minimum number typically  
367 recommended for detecting forced multi-decadal signals (e.g., Deser et al., 2012). However, internal variability  
368 cannot be ruled out, and studies have, for example, discussed the association of Atlantic slow-frequency variability  
369 with the ISM multi-decadal mode (e.g., Rajesh and Goswami, 2020). In this context, the use of large single-forcing  
370 ensembles (e.g., Smith et al., 2022; Simpson et al., 2023) offers a promising approach to disentangling the  
371 individual contributions of greenhouse gases, anthropogenic aerosols and other external drivers. Furthermore, our  
372 findings are based on a single climate model and therefore depend on its representation of aerosol-cloud-radiation  
373 and circulation interactions. Given the well-known uncertainties in aerosol forcing and its climatic effects, the  
374 response may differ across models and from real-world observations. For example, CESM1 is known to exhibit a  
375 relatively strong aerosol effective radiative forcing (Zelinka et al., 2014; 2023), which may result in a stronger  
376 climate response to aerosol perturbations than seen in other models.

377

378 **Acknowledgements.** MAB acknowledges support from the Natural Environment Research Council  
379 (NE/N006038/1) and the Research Council of Norway (grant no. 324182; CATHY).

380

381 **Data availability.** GPCC data are retrieved from <https://psl.noaa.gov/data/gridded/data.gpcc.html>, CRU data from  
382 <https://crudata.uea.ac.uk/cru/data/hrg/>, and UDEL data from  
383 [https://psl.noaa.gov/data/gridded/data.UDel\\_AirT\\_Precip.html](https://psl.noaa.gov/data/gridded/data.UDel_AirT_Precip.html). The ERA5 data are obtained at  
384 <https://cds.climate.copernicus.eu/datasets/reanalysis-era5-pressure-levels-monthly-means>. HadISST data are  
385 available from <https://www.metoffice.gov.uk/hadobs/hadisst/>, while the HadSLP2 dataset is accessed from  
386 <https://www.metoffice.gov.uk/hadobs/hadslp2/>. The CESM model data used in this study are available from MAB  
387 upon request.

388

389 **Author contribution.** WS and MAB designed the study. WS performed the analysis and completed the first draft  
390 of the manuscript. WS and MAB discussed the results, WA, MAB, and IC edited the manuscript. GW and YL  
391 provided suggestions on the analysis and interpretation of the results.

392

393 **Competing interests.** The authors have no competing interests to declare.

394

395 **References**

- 396 Allan, R., and Ansell, T.: A New Globally Complete Monthly Historical Gridded Mean Sea Level Pressure Dataset  
397 (HadSLP2): 1850–2004, *J. Climate*, 19, <https://doi.org/10.1175/JCLI3937.1>, 2006.
- 398 Andrews, T., and Forster, P.M.: Energy budget constraints on historical radiative forcing, *Nat. Clim. Chang.* 10,  
399 <https://doi.org/10.1038/s41558-020-0696-1>, 2020.
- 400 Bartlett, R. E., Bollasina, M. A., Booth, B. B. B. et al.: Do differences in future sulfate emission pathways matter  
401 for near-term climate? A case study for the Asian monsoon, *Clim. Dynam.*, 50, [https://doi.org/10.1007/s00382-](https://doi.org/10.1007/s00382-017-3726-6)  
402 [017-3726-6](https://doi.org/10.1007/s00382-017-3726-6), 2018.
- 403 Bellouin, N., et al.: Bounding aerosol radiative forcing of climate change, *Rev. Geophys.*, 58,  
404 <https://doi.org/10.1029/2019RG000660>, 2020.
- 405 Bollasina, M.A, Ming, Y, Ramaswamy, V.: Anthropogenic aerosols and the weakening of the South Asian summer  
406 monsoon, *Science*, 334, <https://doi.org/10.1126/science.1204994>, 2011.
- 407 Bollasina, M. A., Ming, Y., Ramaswamy, V., Schwarzkopf, M. D., and Naik, V.: Contribution of local and remote  
408 anthropogenic aerosols to the twentieth century weakening of the South Asian monsoon, *Geophys. Res. Lett.*,  
409 41, <https://doi.org/10.1002/2013GL058183>, 2014.
- 410 Boucher, O., Randall, D., Artaxo, P., Bretherton, C., Feingold, G., Forster, P., Kerminen, V.-M., Kondo, Y., Liao,  
411 H., Lohmann, U., Rasch, P., Satheesh, S., Sherwood, S., Stevens, B., and Zhang, X.: Clouds and aerosols, in  
412 *Climate change 2013: The physical science basis. Contribution of Working Group I to the Fifth Assessment*  
413 *Report of the Intergovernmental Panel on Climate Change*, edited by Stocker T., Qin D., Plattner G.-K., Tignor  
414 M., Allen S., Boschung J., Nauels A., Xia Y., Bex V., and Midgley P., chap. 7, pp. 571–658, Cambridge  
415 University Press, Cambridge, United Kingdom and New York, NY, USA,  
416 <https://10.1017/CBO9781107415324.016>, 2013.
- 417 Cowan, T. and Cai, W.: The impact of Asian and non-Asian anthropogenic aerosols on 20th century Asian summer  
418 monsoon, *Geophys. Res. Lett.*, 38, <https://doi.org/10.1029/2011GL047268>, 2011.
- 419 Deser, C., Phillips, A., Bourdette, V., et al.: Uncertainty in climate change projections: the role of internal  
420 variability, *Clim. Dynam.*, 38, <https://doi.org/10.1007/s00382-010-0977-x>, 2012.
- 421 Dong, B., Sutton, R. T., Highwood, E. J., and Wilcox, L. J.: Preferred response of the East Asian summer monsoon  
422 to local and non-local anthropogenic sulphur dioxide emissions, *Clim. Dynam.*, 46,  
423 <https://doi.org/10.1007/s00382-015-2671-5>, 2016.

424 Dong, B., Wilcox, L.J., Highwood, E.J., and Sutton, R. T.: Impacts of recent decadal changes in Asian aerosols on  
425 the East Asian summer monsoon: roles of aerosol–radiation and aerosol–cloud interactions, *Clim. Dynam.*,  
426 53, <https://doi.org/10.1007/s00382-019-04698-0>, 2019.

427 Enomoto, T., Hoskins, B.J., and Matsuda, Y.: The formation mechanism of the Bonin high in August, *Q. J. Roy.*  
428 *Meteor. Soc.*, 129, <https://doi.org/10.1256/qj.01.211>, 2003.

429 Gadgil, S., and Rupa Kumar, K.: The Asian monsoon — agriculture and economy. In: *The Asian Monsoon*.  
430 Springer Praxis Books. Springer, Berlin, Heidelberg. [https://doi.org/10.1007/3-540-37722-0\\_18](https://doi.org/10.1007/3-540-37722-0_18), 2006.

431 Ghan, S. J., Liu, X., Easter, R. C., Zaveri, R., Rasch, P. J., et al.: Toward a minimal representation of aerosols in  
432 climate models: Comparative decomposition of aerosol direct, semidirect, and indirect radiative forcing, *J.*  
433 *Climate*, 25, <https://doi.org/10.1175/JCLI-D-11-00650.1>, 2012.

434 Goswami, D. J., Ashok, K., and Goswami, B. N.: Local ocean–atmosphere interaction in Indian summer monsoon  
435 multi-decadal variability, *Clim. Dynam.*, 60, <https://doi.org/10.1007/s00382-022-06377-z>, 2023.

436 Guo, L., Highwood, E. J., Shaffrey, L. C., and Turner, A. G.: The effect of regional changes in anthropogenic  
437 aerosols on rainfall of the East Asian summer monsoon, *Atmos. Chem. Phys.*, 13, [https://doi.org/10.5194/acp-](https://doi.org/10.5194/acp-13-1521-2013)  
438 [13-1521-2013](https://doi.org/10.5194/acp-13-1521-2013), 2013.

439 Guo, L., Turner, A. G., and Highwood, E. J.: Impacts of 20<sup>th</sup> century aerosol emissions on the South Asian  
440 monsoon in the CMIP5 models, *Atmos. Chem. Phys.*, 15, <https://doi.org/10.5194/acp-15-6367-2015>, 2015.

441 Harris, I., Jones, P.D., Osborn, T.J. and Lister, D.H.: Updated high-resolution grids of monthly climatic  
442 observations – the CRU TS3.10 Dataset, *Int. J. Climatol.*, 34, <https://doi.org/10.1002/joc.3711>, 2014.

443 He, L., Zhou, T., and Chen, X.: South Asian summer rainfall from CMIP3 to CMIP6 models: biases and  
444 improvements, *Clim. Dynam.*, 61, <https://doi.org/10.1007/s00382-022-06542-4>, 2023.

445 Hegerl G.C., Bronnimann S., et al.: Causes of climate change over the historical record, *Environ. Res. Lett.*, 14,  
446 <https://doi.org/10.1088/1748-9326/ab4557>, 2019.

447 Hersbach, H., Bell, B., Berrisford, P., et al.: The ERA5 global reanalysis. *Q. J. Roy. Meteor. Soc.*, 146,  
448 <https://doi.org/10.1002/qj.3803>, 2020.

449 Hoesly, R.M., et al.: Historical (1750–2014) anthropogenic emissions of reactive gases and aerosols from the  
450 Community Emissions Data System (CEDS), *Geosci. Model Dev.*, 11, [https://doi.org/10.5194/gmd-11-369-](https://doi.org/10.5194/gmd-11-369-2018)  
451 [2018](https://doi.org/10.5194/gmd-11-369-2018), 2018.

452 Huang, X., and Coauthors: The recent decline and recovery of Indian summer monsoon rainfall: relative roles of

453 external forcing and internal variability, *J. Climate*, 33, <https://doi.org/10.1175/JCLI-D-19-0833.1>, 2020.

454 Hurrell, J. W., Holland, M. M., Gent, P. R., Ghan, S., Kay, J. E., et al.: The Community Earth System Model, *Bull.*  
455 *Amer. Met. Soc.*, 94, <https://doi.org/10.1175/BAMS-D-12-00121.1>, 2013.

456 Koffi, B., Dentener, F., Janssens-Maenhout, G., Guizzardi, D., Crippa, M., et al.: Hemispheric transport air  
457 pollution (HTAP): Specification of the HTAP2 experiments ensuring harmonized modelling (Tech. rep.)  
458 Luxembourg: Joint Research Centre JRC. <https://doi.org/10.2788/725244>, 2016.

459 Lau, W.K.M.: The aerosol-monsoon climate system of Asia: A new paradigm, *J. Meteor. Res.*, 30,  
460 <https://doi.org/10.1007/s13351-015-5999-1>, 2016.

461 Li, X., Li, Q., Ding, Y., Yang, S., et al.: Possible influence of the interdecadal variation of the extratropical southern  
462 Indian Ocean SST on East Asian summer monsoon precipitation, *Atmos. Res.*, 288,  
463 <https://doi.org/10.1016/j.atmosres.2023.106721>, 2023.

464 Li, X., Ting, M., Li, C., and Henderson, N.: Mechanisms of Asian summer monsoon changes in response to  
465 anthropogenic forcing in CMIP5 models, *J. Climate*, 28, <https://doi.org/10.1175/JCLI-D-14-00559.1>, 2015.

466 Li, Z., et al.: Aerosol and monsoon climate interactions over Asia, *Rev. Geophys.*, 54,  
467 <https://doi.org/10.1002/2015RG000500>, 2016.

468 Li, J., Carlson, B.E., Yung, Y.L., et al.: Scattering and absorbing aerosols in the climate system, *Nat. Rev. Earth*  
469 *Environ.*, 3, <https://doi.org/10.1038/s43017-022-00296-7>, 2022.

470 Liu, L., Shawki, D., Voulgarakis, A., Kasoar, M., Samset, B. H., et al.: A PDRMIP Multimodel study on the  
471 impacts of regional aerosol forcings on global and regional precipitation, *J. Climate*, 31,  
472 <https://doi.org/10.1175/JCLI-D-17-0439.1>, 2018.

473 Liu, Y., Cai, W., Sun, C., Song, H., Cobb, K. M., et al.: Anthropogenic aerosols cause recent pronounced  
474 weakening of Asian summer monsoon relative to last four centuries, *Geophys. Res. Lett.*, 46, 5469–5479,  
475 <https://doi.org/10.1029/2019GL082497>, 2019.

476 Liu, Z., Bollasina, M. A., and Wilcox, L. J.: Impact of Asian aerosols on the summer monsoon strongly modulated  
477 by regional precipitation biases, *Atmos. Chem. Phys.*, 24, 7227–7252, [https://doi.org/10.5194/acp-24-7227-](https://doi.org/10.5194/acp-24-7227-2024)  
478 [2024](https://doi.org/10.5194/acp-24-7227-2024), 2024.

479 Lu, R.-Y., Oh, J.H., and Kim, B.J.: A teleconnection pattern in upper-level meridional wind over the North African  
480 and Eurasian continent in summer, *Tellus A*, 54, <https://doi.org/10.3402/tellusa.v54i1.12122>, 2002.

481 Lund, M. T., Myhre, G., and Samset, B. H.: Anthropogenic aerosol forcing under the Shared Socioeconomic

482 Pathways, Atmos. Chem. Phys., 19, <https://doi.org/10.5194/acp-19-13827-2019>, 2019.

483 Meehl, G. A., and Arblaster, J. M.: GCM sensitivity experiments for the Indian monsoon and tropospheric biennial  
484 oscillation transition conditions, J. Climate, 15, [https://doi.org/10.1175/1520-0442\(2002\)015<0923:imgset>2.0.co;2](https://doi.org/10.1175/1520-0442(2002)015<0923:imgset>2.0.co;2), 2002.

486 Meehl, G.A., Shields, C., Arblaster, J.M., Annamalai, H., and Neale, R.: Intraseasonal, seasonal, and interannual  
487 characteristics of regional monsoon simulations in CESM2, J. Adv. Model. Earth Sys., 12,  
488 <https://doi.org/10.1029/2019MS001962>, 2020.

489 Meehl, G. A., Shields, C. A., Arblaster, J. M., Fasullo, J., Rosenbloom, N., Hu, A., et al.: Processes that contribute  
490 to future South Asian monsoon differences in E3SMv2 and CESM2, Geophys. Res. Lett., 51,  
491 <https://doi.org/10.1029/2024GL109056>, 2024.

492 Neale, R. B., Gettelman, A., Park, S., Chen, C.-C., Lauritzen, P. H., et al.: Description of the NCAR Community  
493 Atmosphere Model (CAM 5.0), NCAR technical note, NCAR/TN-48, 274.  
494 <https://doi.org/10.5065/D6N877R0>, 2012.

495 Persad, G., Samset, B.H., Wilcox, L.J., Allen, R.J., Bollasina, M.A., et al.: Rapidly evolving aerosol emissions are  
496 a dangerous omission from near-term climate risk assessments, Environ. Res. Climate, 2,  
497 <https://doi.org/10.1088/2752-5295/acd6af>, 2023.

498 Preethi, B., Mujumdar, M., Kripalani, R.H. et al.: Recent trends and tele-connections among South and East Asian  
499 summer monsoons in a warming environment, Clim. Dynam., 48, [https://doi.org/10.1007/s00382-016-3218-](https://doi.org/10.1007/s00382-016-3218-0)  
500 [0](https://doi.org/10.1007/s00382-016-3218-0), 2017.

501 Rajesh, P. V., and Goswami, B. N.: Four-dimensional structure and sub-seasonal regulation of the Indian summer  
502 monsoon multi-decadal mode, Clim. Dynam., 55, <https://doi.org/10.1007/s00382-020-05407-y>, 2020.

503 Rao, S.A., Dhakate, A.R., Saha, S.K. et al.: Why is Indian Ocean warming consistently?, Climatic Change, 110,  
504 <https://doi.org/10.1007/s10584-011-0121-x>, 2012.

505 Rayner, N. A., Parker, D. E., Horton, E. B., Folland, C. K., Alexander, L. V., Rowell, D. P., Kent, E. C., and  
506 Kaplan, A.: Global analyses of sea surface temperature, sea ice, and night marine air temperature since the late  
507 nineteenth century, J. Geophys. Res., 108, <https://doi.org/10.1029/2002JD002670>, 2003.

508 Rodwell, M. J., and Hoskins, B. J.: Subtropical anticyclones and summer monsoons, J. Climate, 14,  
509 [https://doi.org/10.1175/1520-0442\(2001\)014<3192:SAASM>2.0.CO;2](https://doi.org/10.1175/1520-0442(2001)014<3192:SAASM>2.0.CO;2), 2001.

510 Roxy, M. K., Ritika, K., Terray, P., and Masson, S.: The curious case of Indian Ocean warming. J. Climate, 27,

511 <https://doi.org/10.1175/JCLI-D-14-00471.1>, 2014.

512 Roxy, M., Ritika, K., Terray, P. et al.: Drying of Indian subcontinent by rapid Indian Ocean warming and a  
513 weakening land-sea thermal gradient, *Nat. Commun.*, 6, <https://doi.org/10.1038/ncomms8423>, 2015.

514 Saha, A., and Ghosh, S.: Can the weakening of the Indian Monsoon be attributed to anthropogenic aerosols?  
515 *Environ. Res. Commun.*, 1, <https://doi:10.1088/2515-7620/ab2c65>, 2019.

516 Salzmann, M., Weser, H., Cherian, R.: Robust response of Asian summer monsoon to anthropogenic aerosols in  
517 CMIP5 models, *J. Geophys. Res. Atmos.*, 119, <https://doi:10.1002/2014JD021783>, 2014.

518 Salzmann, M., and Cherian, R.: On the enhancement of the Indian summer monsoon drying by Pacific  
519 multidecadal variability during the latter half of the twentieth century, *J. Geophys. Res. Atmos.*, 120,  
520 <https://doi:10.1002/2015JD023313>, 2015.

521 Samset, B. H., et al.: Climate impacts from a removal of anthropogenic aerosol emissions. *Geophys. Res. Lett.*,  
522 45, <https://doi.org/10.1002/2017GL076079>, 2018.

523 Samset, B.H., Lund, M.T., Bollasina, M., et al.: Emerging Asian aerosol patterns. *Nat. Geosci.*, 12,  
524 <https://doi.org/10.1038/s41561-019-0424-5>, 2019.

525 Schneider, U., Becker, A., Finger, P. et al.: GPCP's new land surface precipitation climatology based on quality-  
526 controlled in situ data and its role in quantifying the global water cycle, *Theor. Appl. Climatol.*, 115,  
527 <https://doi.org/10.1007/s00704-013-0860-x>, 2014,

528 Shao, Z., Wang, H., Geng, Y.F., et al.: East Asian summer monsoon response to anthropogenic aerosols  
529 redistribution: contrasting 1950–1980 and 1980–2010 to understand the role of non-Asian forcing, *Clim.*  
530 *Dynam.*, 62, <https://doi.org/10.1007/s00382-023-07016-x>, 2024.

531 Shawki, D., Voulgarakis, A., Chakraborty, A., Kasoar, M., and Srinivasan, J.: The South Asian monsoon response  
532 to remote aerosols: Global and regional mechanisms, *J. Geophys. Res.*, 123,  
533 <https://doi.org/10.1029/2018JD028623>, 2018.

534 Simpson, I. R., and Coauthors: The CESM2 single-forcing large ensemble and comparison to CESM1:  
535 implications for experimental design. *J. Climate*, 36, <https://doi.org/10.1175/JCLI-D-22-06666.1>, 2023.

536 Smith, S. J., van Aardenne, J., Klimont, Z., Andres, R. J., Volke, A., and Delgado Arias, S.: Anthropogenic sulfur  
537 dioxide emissions: 1850–2005, *Atmos. Chem. Phys.*, 11, <https://doi.org/10.5194/acp-11-1101-2011>, 2011.

538 Smith, D., Gillett, N. P., Simpson, I. R., Athanasiadis, P. J., Baehr, J., Bethke, I., et al.: Attribution of multi-annual  
539 to decadal changes in the climate system: The large ensemble single forcing model intercomparison project

540 (LESMIP), *Front. Clim.*, 4, <https://doi.org/10.3389/fclim.2022.955414>, 2022.

541 Song, F., Zhou, T., and Qian, Y.: Responses of East Asian summer monsoon to natural and anthropogenic forcings  
542 in the 17 latest CMIP5 models, *Geophys. Res. Lett.*, 41, <https://doi.org/10.1002/2013GL058705>, 2014.

543 Stier, P., van den Heever, S.C., Christensen, M.W., et al.: Multifaceted aerosol effects on precipitation, *Nat.*  
544 *Geosci.*, 17, <https://doi.org/10.1038/s41561-024-01482-6>, 2024.

545 Swapna, P., Krishnan, R., and Wallace, J.M: Indian Ocean and monsoon coupled interactions in a warming  
546 environment, *Clim. Dynam.*, 42, <https://doi.org/10.1007/s00382-013-1787-8>, 2014.

547 Szopa, S., et al.: Short-Lived Climate Forcers. In *Climate Change 2021: The Physical Science Basis. Contribution*  
548 *of Working Group I to the Sixth Assessment Report of the Intergovernmental Panel on Climate Change*  
549 [Masson-Delmotte, V., P. Zhai, A. Pirani, S.L. Connors, C. Péan, S. Berger, N. Caud, Y. Chen, L. Goldfarb,  
550 M.I. Gomis, M. Huang, K. Leitzell, E. Lonnoy, J.B.R. Matthews, T.K. Maycock, T. Waterfield, O. Yelekçi, R.  
551 Yu, and B. Zhou (eds.)]. Cambridge University Press, Cambridge, United Kingdom and New York, NY, USA,  
552 pp. 817–922, <https://doi.org/10.1017/9781009157896.008>, 2021.

553 Takaya, K., and Nakamura, H.: A formulation of a phase-independent wave-activity flux for stationary and  
554 migratory quasigeostrophic eddies on a zonally varying basic flow, *J. Atmos. Sci.*, 58,  
555 [https://doi.org/10.1175/1520-0469\(2001\)058<0608:AFOAPI>2.0.CO;2](https://doi.org/10.1175/1520-0469(2001)058<0608:AFOAPI>2.0.CO;2), 2001.

556 Turner, A., and Annamalai, H.: Climate change and the South Asian summer monsoon, *Nature Clim. Change* 2,  
557 <https://doi.org/10.1038/nclimate1495>, 2012

558 Undorf, S., Bollasina, M., Booth, B., and Hegerl, G.: Contrasting the effects of the 1850-1975 increase in sulphate  
559 aerosols from North America and Europe on the Atlantic in the CESM, *Geophys. Res. Lett.*, 45,  
560 <https://doi.org/10.1029/2018GL079970>, 2018.

561 Undorf, S., Polson, D., Bollasina, M. A., Ming, Y., Schurer, A., and Hegerl, G. C.: Detectable impact of local and  
562 remote anthropogenic aerosols on the 20th century changes of West African and South Asian monsoon  
563 precipitation, *J. Geophys. Res.*, 123, <https://doi.org/10.1029/2017JD027711>, 2018.

564 Wang, Q., Wang, Z., and Zhang, H.: Impact of anthropogenic aerosols from global, East Asian, and non-East  
565 Asian sources on East Asian summer monsoon system, *Atmos. Res.*, 183,  
566 <https://doi.org/10.1016/j.atmosres.2016.08.023>, 2017.

567 Wang, B., and Coauthors: Toward predicting changes in the land monsoon rainfall a decade in advance. *J. Climate*,  
568 31, <https://doi.org/10.1175/JCLI-D-17-0521.1>, 2018.

569 Wang, Z., Mu, J., Yang, M., and Yu, X.: Reexamining the mechanisms of East Asian summer monsoon changes  
570 in response to non–East Asian anthropogenic aerosol forcing. *J. Climate*, 33, [https://doi.org/10.1175/JCLI-D-](https://doi.org/10.1175/JCLI-D-19-0550.1)  
571 [19-0550.1](https://doi.org/10.1175/JCLI-D-19-0550.1), 2020.

572 Wang, Z., Lin, L., Xu, Y., et al.: Incorrect Asian aerosols affecting the attribution and projection of regional climate  
573 change in CMIP6 models, *npj Clim. Atmos. Sci.*, 4, <https://doi.org/10.1038/s41612-020-00159-2>, 2021.

574 Wang, Z., Feng, J., Diao, C., Li, Y., Lin, L., and Xu, Y.: Reduction in European anthropogenic aerosols and the  
575 weather conditions conducive to PM<sub>2.5</sub> pollution in North China: a potential global teleconnection pathway,  
576 *Environ. Res. Lett.*, 16, <https://doi.org/10.1088/1748-9326/ac269d>, 2021.

577 Watanabe, M.: Asian jet waveguide and a downstream extension of the North Atlantic Oscillation, *J. Climate*, 17,  
578 <https://doi.org/10.1175/JCLI-3228.1>, 2004.

579 Westervelt, D. M., Conley, A. J., Fiore, A. M., Lamarque, J.-F., Shindell, D. T., Previdi, M., Mascioli, N. R.,  
580 Faluvegi, G., Correa, G., and Horowitz, L. W.: Connecting regional aerosol emissions reductions to local and  
581 remote precipitation responses, *Atmos. Chem. Phys.*, 18, 12461–12475, [https://doi.org/10.5194/acp-18-](https://doi.org/10.5194/acp-18-12461-2018)  
582 [12461-2018](https://doi.org/10.5194/acp-18-12461-2018), 2018.

583 Wilcox, L. J., Allen, R. J., Samset, B. H., Bollasina, M. A., et al.: The Regional Aerosol Model Intercomparison  
584 Project (RAMIP), *Geosci. Model Dev.*, 16, <https://doi.org/10.5194/gmd-16-4451-2023>, 2023.

585 Wilcox L. J., Liu, Z., Samset, B. H., et al.: Accelerated increases in global and Asian summer monsoon  
586 precipitation from future aerosol reductions, *Atmos. Chem. Phys.*, 20, [https://doi.org/10.5194/acp-20-11955-](https://doi.org/10.5194/acp-20-11955-2020)  
587 [2020](https://doi.org/10.5194/acp-20-11955-2020), 2020.

588 Willmott, C. J., and Matsuura, K.: Smart interpolation of annually averaged air temperature in the United States,  
589 *J. Appl. Meteor. Climatol.*, 34, [https://doi.org/10.1175/1520-0450\(1995\)034<2577:SIOAAA>2.0.CO;2](https://doi.org/10.1175/1520-0450(1995)034<2577:SIOAAA>2.0.CO;2),  
590 1995.

591 Wu, G. X., Li, Z. Q., Fu, C. B., Zhang, X. Y., Zhang, R. Y., Zhang, R. H., et al.: Advances in studying interactions  
592 between aerosols and monsoon in China. *Science China Earth Sciences*, 59, [https://doi.org/10.1007/s11430-](https://doi.org/10.1007/s11430-015-5198-z)  
593 [015-5198-z](https://doi.org/10.1007/s11430-015-5198-z), 2016.

594 Xiang, B., Xie, S. P., Kang, S. M. et al.: An emerging Asian aerosol dipole pattern reshapes the Asian summer  
595 monsoon and exacerbates northern hemisphere warming, *npj Clim. Atmos. Sci.*, 6,  
596 <https://doi.org/10.1038/s41612-023-00400-8>, 2023.

597 Xie, P., and Arkin, P. A.: Global precipitation: A 17-Year monthly analysis based on gauge observations, satellite

598 estimates, and numerical model outputs, *Bull. Amer. Meteor. Soc.*, 78, <https://doi.org/10.1175/1520->  
599 [0477\(1997\)078<2539:GPAYMA>2.0.CO;2](https://doi.org/10.1175/1520-0477(1997)078<2539:GPAYMA>2.0.CO;2), 1997.

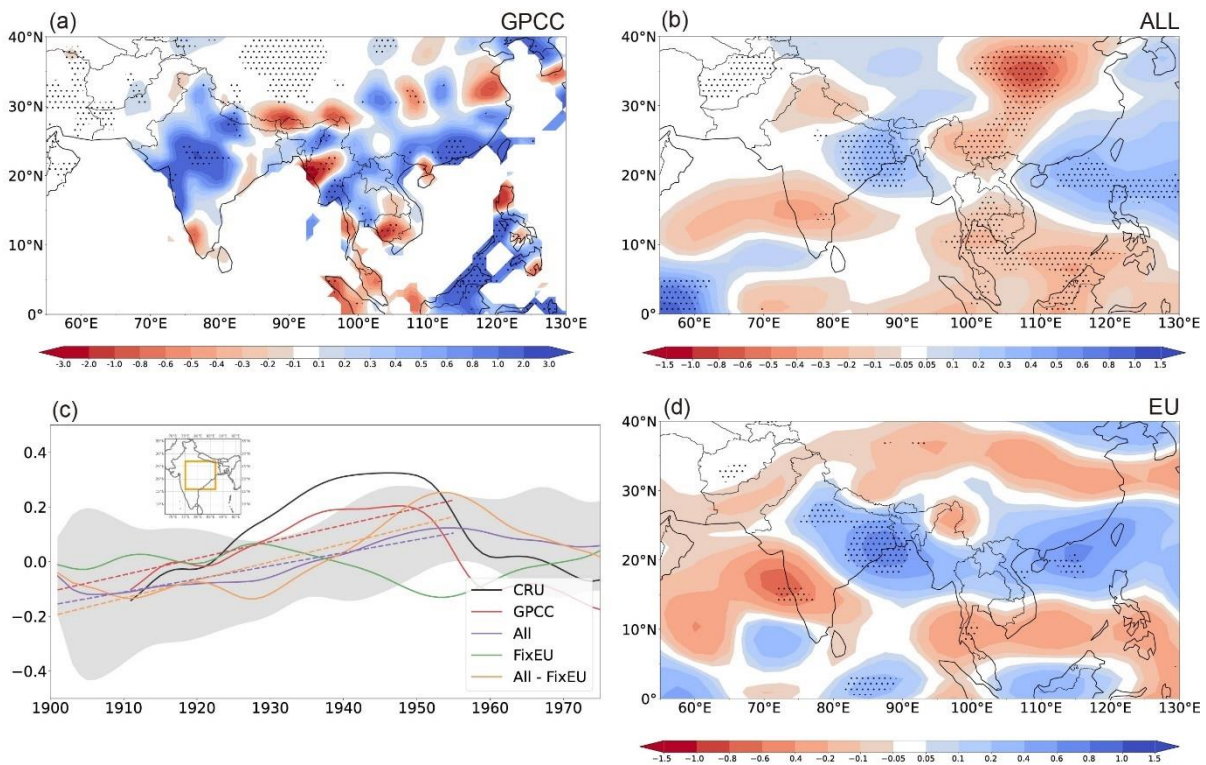
600 Zelinka, M. D., Andrews, T., Forster, P. M., and Taylor, K. E.: Quantifying components of aerosol-cloud-radiation  
601 interactions in climate models, *J. Geophys. Res. Atmos.*, 119, <https://doi.org/10.1002/2014JD021710>, 2014.

602 Zelinka, M. D., Smith, C. J., Qin, Y., and Taylor, K. E.: Comparison of methods to estimate aerosol effective  
603 radiative forcings in climate models, *Atmos. Chem. Phys.*, 23, <https://doi.org/10.5194/acp-23-8879-2023>,  
604 2023.

605 Zhang, L., and Zhou, T.: An assessment of monsoon precipitation changes during 1901–2001. *Clim. Dynam.*, 37,  
606 <https://doi.org/10.1007/s00382-011-0993-5>, 2011.

607

608 **Figures**  
609



610

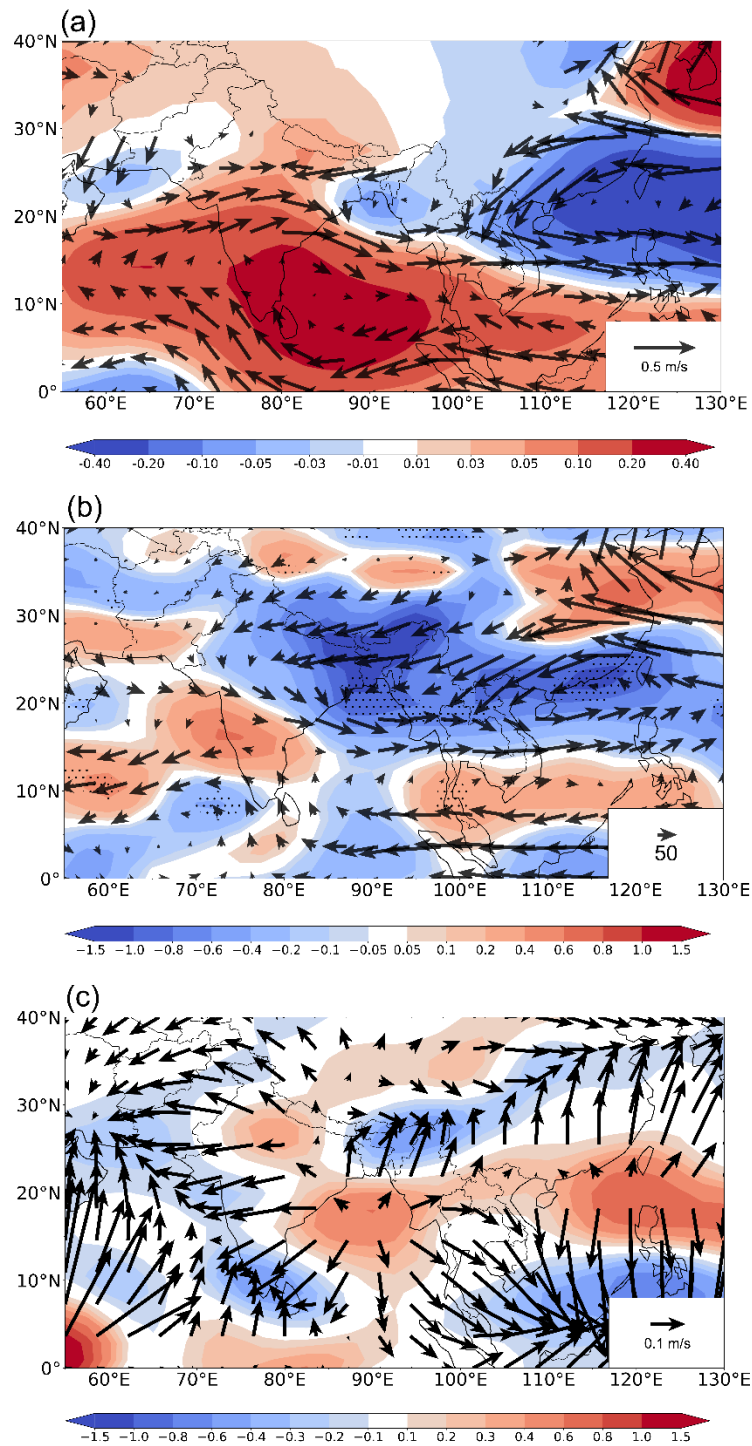
611

612 **Figure 1.** (a)-(b): Spatial patterns of the 1901-1955 linear trends of JJA precipitation ( $\text{mm day}^{-1} (55 \text{ years})^{-1}$ ) for  
613 (a) GPCC, (b) the all-forcing ensemble (ALL), and (d) the difference between ALL and the all-forcing experiment  
614 with fixed preindustrial aerosol emissions over Europe (fixEU), representing the impact of EU aerosols. The black  
615 dots mark the grid points for which the trend exceeds the 90% significance level according to the two-tailed  
616 Student's t-test. (c): Time series of area-averaged JJA precipitation anomalies ( $\text{mm day}^{-1}$ ; deviations from the  
617 1901-2000 climatology) over central-northern India (land-only points within  $75^{\circ}\text{--}87^{\circ}\text{E}$ ,  $16^{\circ}\text{--}27^{\circ}\text{N}$ ; area shown in  
618 inset map) smoothed with 11-year running means to highlight low-frequency (multi-decadal) fluctuations. The  
619 black and red lines represent observations (CRU and GPCC, respectively), while the purple, green and orange  
620 lines represent the ensemble means of ALL, fixEU, and their difference (EU). The grey shading represents the  
621 standard deviation of the eight-member ALL ensemble around the mean. The 1901-1955 least-squares linear  
622 trends of the simulated time series are shown as dashed lines in the corresponding colours. Note that the interval  
623 for the simulated changes is half of that used for the observations.

624

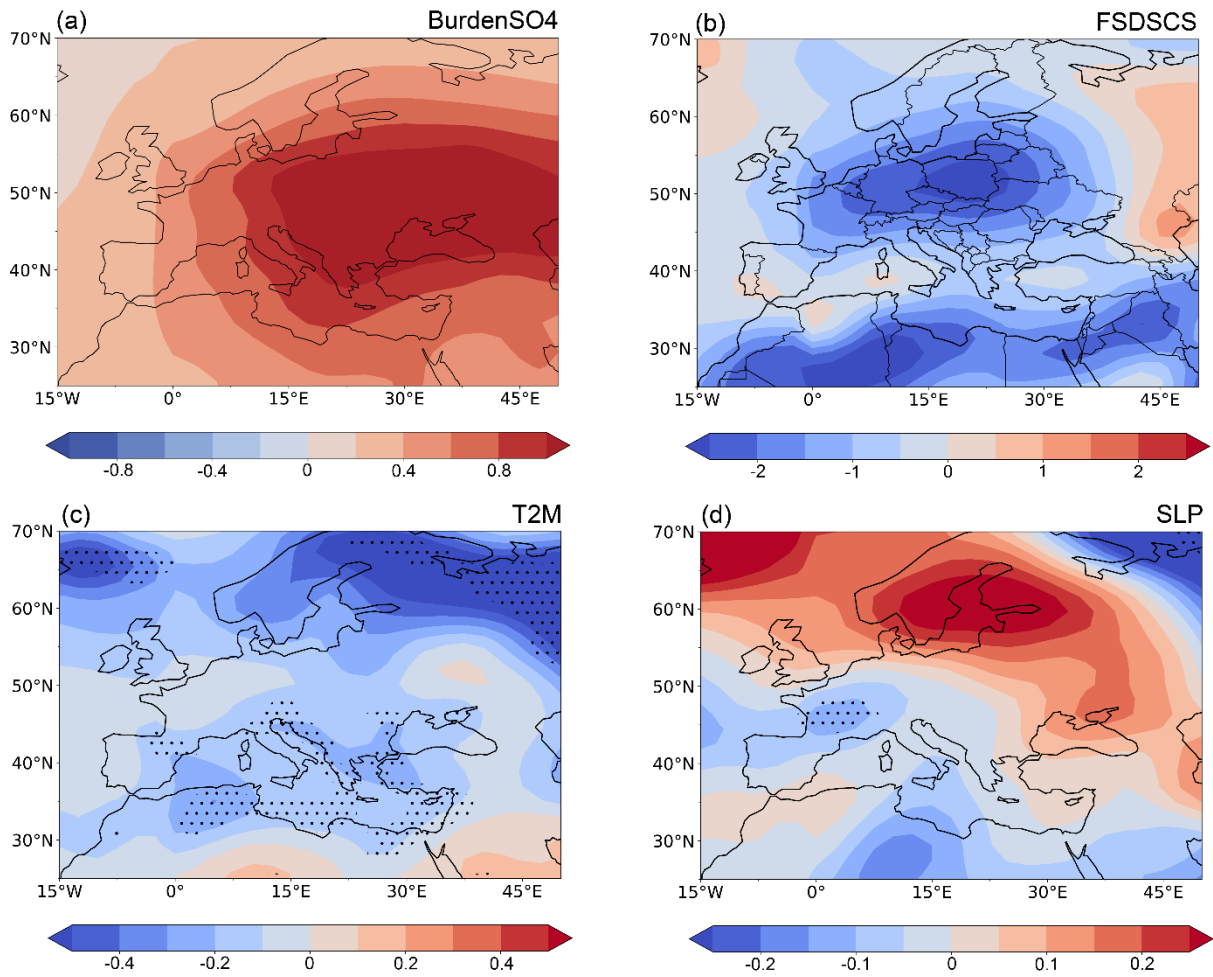
625

626



627

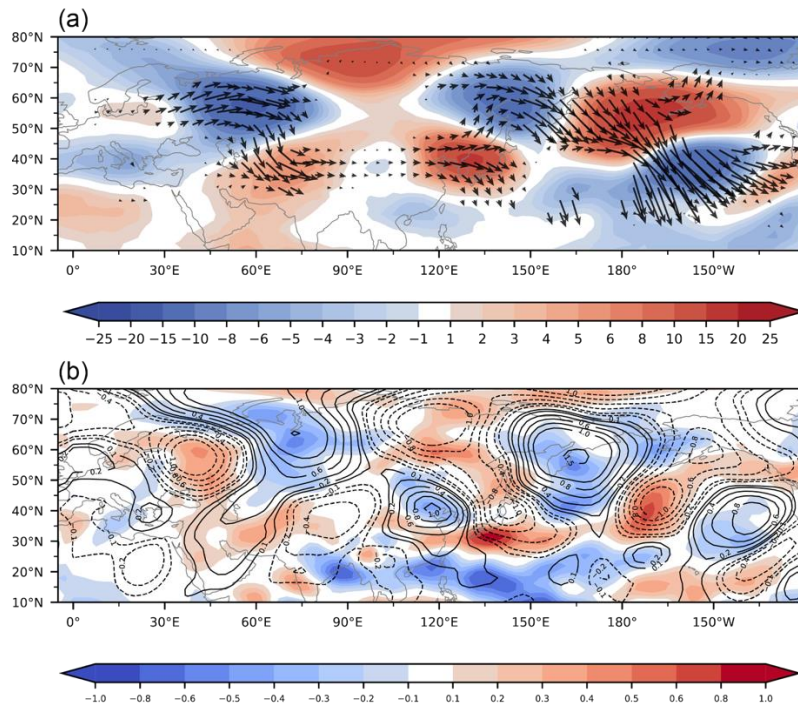
628 **Figure 2.** Spatial patterns of the 1901-1955 linear trends of the JJA average (a) 850-hPa winds ( $\text{m s}^{-1} (55 \text{ years})^{-1}$ ) and 925-hPa streamfunction (colors,  $10^6 \text{ m}^2 \text{ s}^{-1} (55 \text{ years})^{-1}$ ), (b) 1000-300 hPa vertically integrated moisture  
 629 transport (vectors,  $\text{Kg m}^{-1} \text{ s}^{-1}$ ) and its divergence (shades,  $\text{mm d}^{-1} (55 \text{ years})^{-1}$ ), (c) 150-hPa divergent circulation  
 630 ( $\text{m s}^{-1} (55 \text{ years})^{-1}$ ) and its divergence (shades;  $10^{-6} \text{ s}^{-1} (55 \text{ years})^{-1}$ ) associated with increased European sulphate  
 631 aerosols (difference between the ALL and fixEU ensemble means). The black dots in (b) mark the grid points for  
 632 which the trend exceeds the 90% significance level according to the two-tailed Student's t-test.  
 633



635

636

637 **Figure 3.** Spatial patterns of the 1901-1955 linear trends of the JJA average (a) column sulphate aerosol burden  
 638 ( $10^{-5} \text{ kg m}^{-2} (55 \text{ years})^{-1}$ ), (b) surface clear-sky downward shortwave radiation ( $\text{W m}^{-2} (55 \text{ years})^{-1}$ ), (c) 2-m air  
 639 temperature ( $\text{K} (55 \text{ years})^{-1}$ ), and (d) sea level pressure ( $\text{hPa} (55 \text{ years})^{-1}$ ) associated with increased European  
 640 sulphate aerosols (difference between the ALL and fixEU ensemble means). The black dots in (c) and (d) mark  
 641 the grid points for which the trend exceeds the 90% significance level according to the two-tailed Student's t-test.  
 642



644

645

646 **Figure 4.** Spatial patterns of the 1901-1955 linear trends of the JJA average (a) 300-hPa wave activity flux  
 647 (vectors;  $10^{-4} \text{ m}^2 \text{ s}^{-2} (55 \text{ years})^{-1}$ ) and streamfunction (shades;  $10^5 \text{ m}^2 \text{ s}^{-1} (55 \text{ years})^{-1}$ ), and (b) 300-hPa meridional  
 648 wind (contours;  $\text{m s}^{-1} (55 \text{ years})^{-1}$ ) and 500-hPa vertical velocity (shades;  $10^{-2} \text{ Pa s}^{-1} (55 \text{ years})^{-1}$ ) associated with  
 649 increased European sulphate aerosols (difference between the ALL and fixEU ensemble means).